*Int. J. Heat Mass Transfer.* Vol. 7, pp. 1273–1289. Pergamon Press 1964. Printed in Great Britain

# DIRECT-CONTACT HEAT TRANSFER WITH CHANGE OF PHASE: EVAPORATION OF DROPS IN AN IMMISCIBLE LIQUID MEDIUM

**S. SIDEMAN and Y. TAITEL†**

Department of Chemical Engineering, Technion—Israel Institute of Technology, Haifa, Israel

(*Received* 12 *September* 1963 *and in revised form* 19 *March* 1964)

**Abstract**—The transfer characteristics of volatile liquid drops evaporating while rising in a column of another immiscible liquid are presented. A study of ciné-camera films taken during the heat- transfer process rendered information regarding the velocities and evaporation rates of butane and pentane drops evaporating in sea water and distilled water. Overall heat-transfer coefficients related to the initial area of the liquid drop, and instantaneous heat-transfer coefficients related to the actual area are presented. The latter are compared with an analytical study of this problem which yields the equation:

$$Nu = \left(\frac{3\cos\beta - \cos^3\beta + 2}{\pi}\right)^{0.5} Pe^{0.5} = a\,Pe^{0.5}$$

for the average Nusselt number, where $2\beta$ is the opening angle of the vapour phase in the drop. It is suggested that with $\beta = 135°$ ($a = 0{\cdot}27$) good approximation of the maximum heat-transfer coefficients may be obtained.

## NOMENCLATURE

$A$, instantaneous drop area;
$a$, constant, equation (25);
$A_0$, drop area at $t = 0$;
$A^*$, initial drop area (in liquid form);
$B$, experimental constant, equation (28);
$C$, experimental constant, equation (26);
$C_p$, specific heat capacity, [kcal/kg degC];
$D$, drop diameter;
$D^*$, initial drop diameter;
$G$, weight of drop;
$G_v$, weight of vapour phase;
$H$, level of drop above nucleation point;
$H_0$, level of drop at $t = 0$;
$H_v$, level of complete evaporation;
$h$, overall heat-transfer coefficient [kcal/m² h degC];
$h_m^*$, mean overall heat-transfer coefficient referred to initial drop area;
$K$, experimental constant, equation (27);
$k$, thermal conductivity [kcal/m h degC];
$m$, experimental constant, equation (27);
$M$, constant, equation (8);
$Nu$, Nusselt number $[hD/k]$;
$n$, experimental constant, equation (26);
$Pe$, Peclet number $[UD/\alpha]$;
$Pr$, Prandtl number $[\mu Cp/k]$;
$p$, experimental constant, equation (28);
$Q$, heat input [kcal];
$Q_0$, heat capacity of drop at $t = 0$ [kcal];
$Q_{max}$, maximum heat absorbed by drop [kcal];
$q$, heat flux [kcal/m²h];
$q'$, rate of heat flow [kcal/h];
$q_\theta$, local heat flux [kcal/m²h];
$R$, radius of drop;
$Re$, Reynolds number $[UD\rho/\mu]$;
$r$, radial co-ordinate;
$T$, temperature;
$T_0$, reduced boiling-point temperature;
$T_\infty$, temperature, continuous phase, upstream;
$t$, time;
$t_v$, time of complete evaporation;
$U$, relative velocity;

† Present address: Department of Mechanical Engineering, University of Delaware, Newark, Del., U.S.A.

$U_r$, velocity vector, spherical co-ordinate;
$U_\theta$, velocity vector, spherical co-ordinate;
$y$, radial distance from drop [$r - R$].

Greek symbols
$\alpha$, thermal diffusivity [m²/h];
$\beta$, opening half-angle of vapour phase, Fig. 2;
$\delta$, infinitesimal variant;
$\epsilon$, complementary opening angle;
$\theta$, spherical co-ordinate;
$\mu$, viscosity [kg/m-h];
$\xi$, vaporization ratio [$G_V/G$], weight per cent evaporated;
$\rho$, density [kg/m³]
$\varphi$, variable, equation (11);
$\psi$, variable, equation (10).

## INTRODUCTION

DIRECT contact between fluids and their relative motion makes heat (or mass) exchange between them rather effective. The quest for economical water desalination units has recently stimulated research on direct-contact heat exchangers, in which one liquid is dispersed in another immiscible liquid. Although a great number of theoretical and experimental studies have been reported on the transfer mechanism between the drops and the continuous liquid media [1], relatively little has been done or reported on direct-contact heat transfer in which the drops evaporate and cool the continuous liquid phase. Umano [2], Wiegandt [3–5] and others [6] have studied the problem of saline water conversion by direct-contact freezing. These and our own recent studies [7] indicate the following advantages of utilizing a secondary refrigerant in direct-contact heat exchangers: (*a*) an economical (closed) refrigeration cycle is feasible; (*b*) smaller quantities and lower flow rates of the cooling fluid are required; (*c*) larger, more effective heat-transfer areas are obtainable; (*d*) separation of the two fluids is very convenient; (*e*) heat-transfer coefficients are higher by one or two orders of magnitude. However, although some information is available regarding technical and economic aspects of the general problem of water conversion by direct-contact freezing, there is none regarding the basic mechanism and the actual heat-transfer coefficients. The present work constitutes the first step in this direction.

When a drop of volatile liquid is evaporating while completely immersed in another non-volatile immiscible liquid, the vapour forms a spheroid at the upper part of the drop, whereas the remaining volatile liquid concentrates at the bottom part of the spheroid-like drop (Fig. 1). Once nucleation sets in in the rising volatile drop, the rate of vapour-phase growth depends mainly on the temperature difference between the drop and the continuous medium. The various stages of a pentane drop evaporating in water are illustrated in Fig. 2. Note that when 1 per cent (by weight) of the liquid has evaporated, the vapour occupies most of the volume of the drop. Above 10 per cent evaporation the thin liquid layer at the bottom of the drop can no longer be observed.

The results obtained in cinemascopic studies of single drops of butane and pentane evaporating in distilled and sea water are reported. These include (*a*) the height and time required for total evaporation; (*b*) the velocity of rise of evaporating drops; (*c*) the average overall heat-transfer coefficients, $h_m^*$ related to the initial surface of the liquid drop, $A^*$; (*d*) the average overall heat-transfer coefficients, $h$, related to the actual instantaneous area of the drop, $A$. The latter, though not of direct practical value, is most suitable for the physical analysis of this complicated three-phase transfer mechanism.

## THEORETICAL

Using spherical co-ordinates ($r$, $\theta$, $\varphi$), the drop is assumed to be a sphere in which the vapour phase is bounded at the upper end by the opening angle $2\beta$, and the liquid phase at the lower part is bounded by $\epsilon = 360 - 2\beta$ as shown in Fig. 3. It is assumed that there is no heat flux across the surface ($r = R$, $\theta < \beta$), hence $(\partial T/\partial r)_R = 0$. The liquid phase is assumed to be at the boiling point corresponding to the vaporization pressure. The temperature of the continuous medium $T_\infty$ is taken as a reference temperature, i.e. $T_\infty = 0$, and the corresponding reduced temperature of the liquid layer is constant, $T_0$. The drop is assumed to be moving in a potential flow field. The relative motion of the drop with respect to the continuous phase is

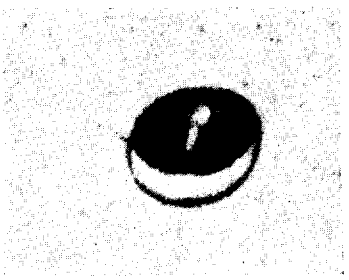

FIG. 1. Butane drop evaporating in sea water (below 1% evaporation).
Picture taken with 16 mm Paillard-Bolex ciné camera.

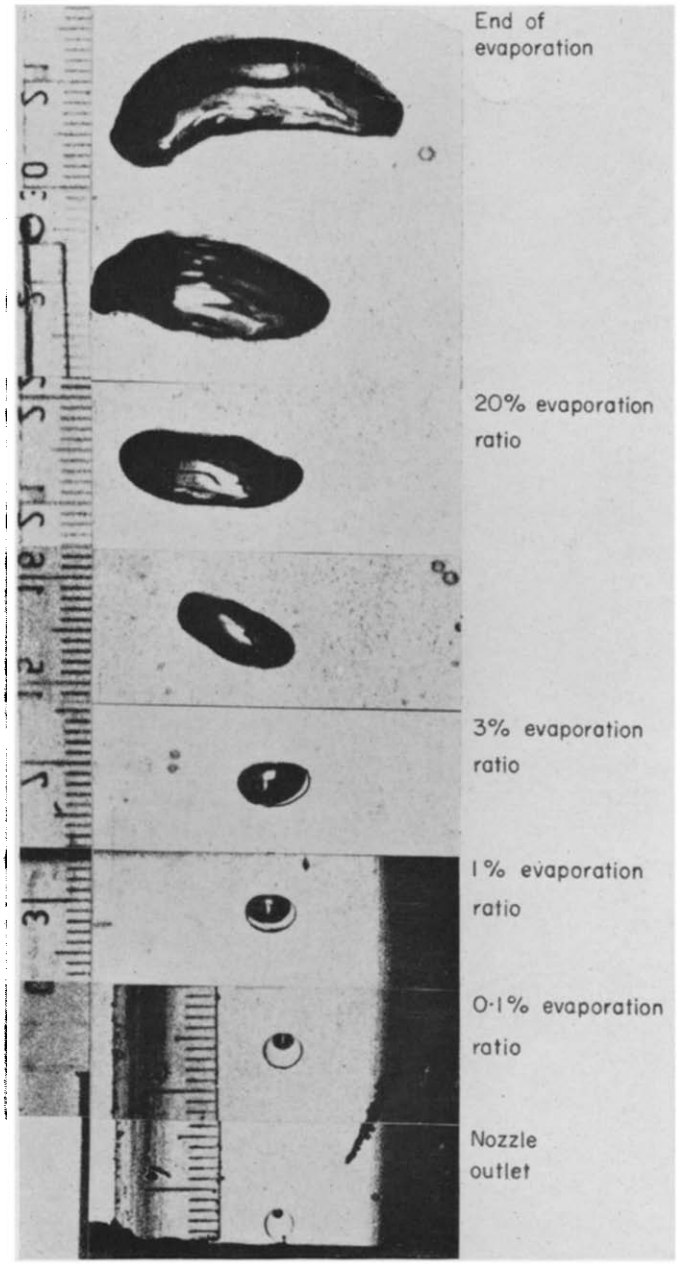


FIG. 2. Pentane drop evaporating in water. 3·5 mm initial drop diameter. Pictures taken with 16 mm Paillard-Bolex H-16 ciné-camera.

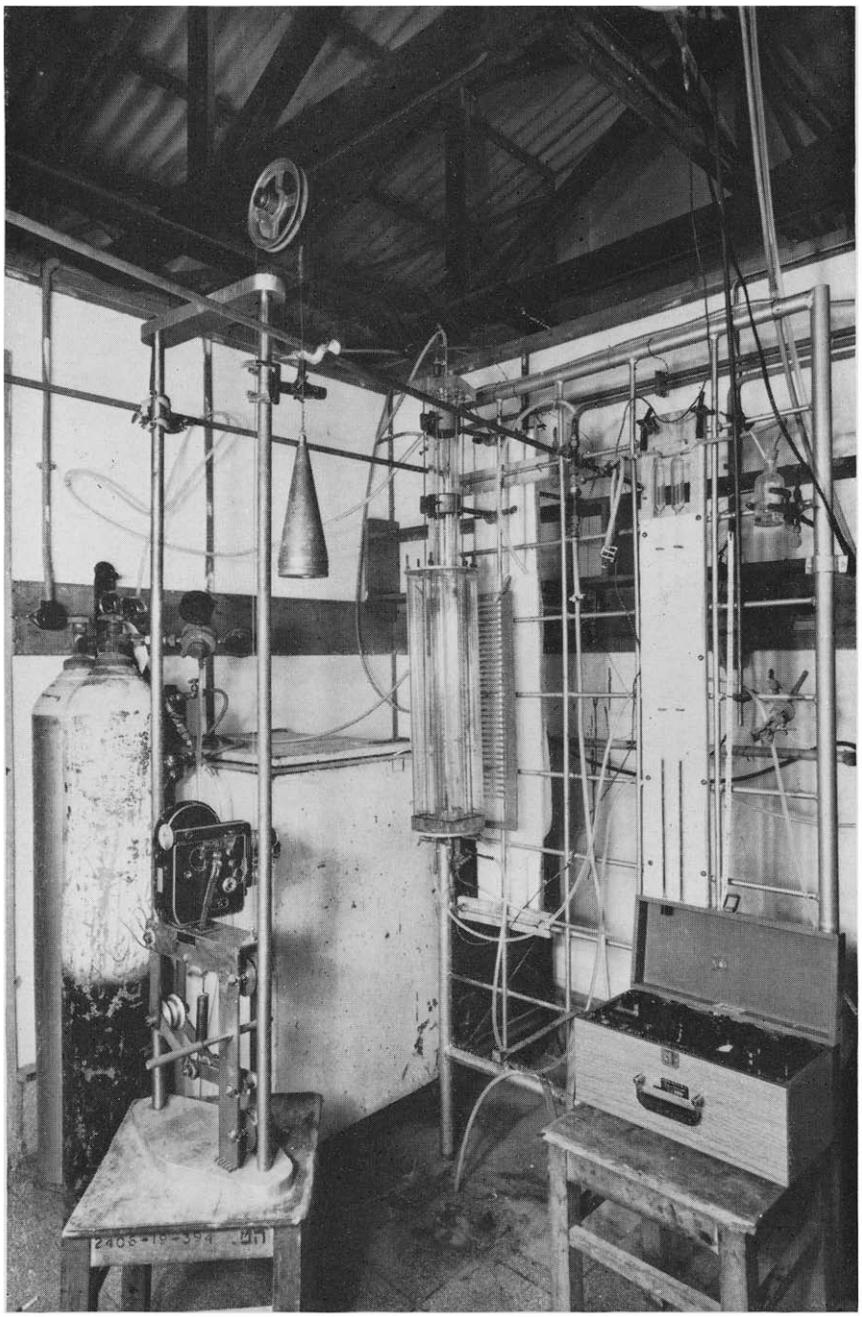

FIG. 6. General picture of apparatus, pentane/water system.

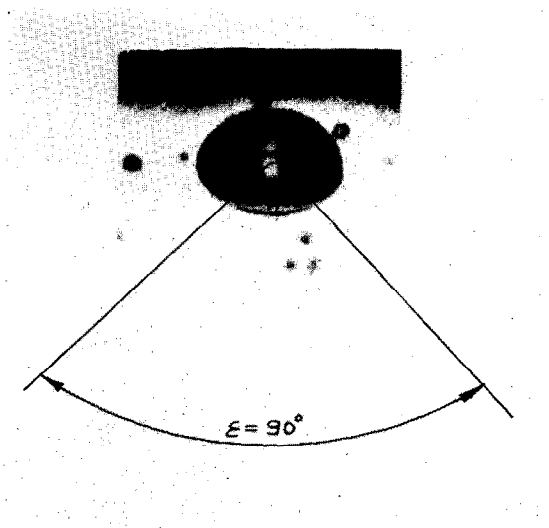


FIG. 18. Experimental vapour opening angle. Pentane drop in sea water, 7·5% evaporation, 2 mm initial drop diameter.

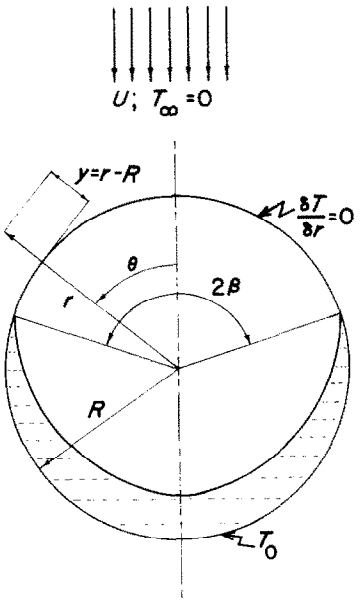


FIG. 3. Analytical model and co-ordinates.

represented by $U$, the downward velocity of the undisturbed continuous medium at $r \to \infty$. The radius of the drop is taken as constant, i.e. the effect of increasing drop diameter is neglected compared with the relative velocity of the drop. The system is in steady-state and axial symmetry exists. Heat transfer takes place in the thin layer of the continuous phase surrounding the drop. Finally, conduction in the $\theta$ direction is assumed negligible compared with convection in the same direction.

The differential equation for steady-state heat transfer with axial symmetry is given by:

$$\underset{\text{I}}{U_r \frac{\partial T}{\partial r}} + \underset{\text{II}}{\frac{U_\theta}{r} \frac{\partial T}{\partial \theta}} = \alpha \left[ \underset{\text{III}}{\frac{1}{r^2} \frac{\partial}{\partial r} \left( r^2 \frac{\partial T}{\partial r} \right)} + \underset{\text{IV}}{\frac{1}{r^2 \sin \theta} \frac{\partial}{\partial \theta} \left( \sin \theta \frac{\partial T}{\partial \theta} \right)} \right] \quad (1)$$

where $\alpha$ is the thermal diffusivity and the velocity vectors are given by:

$$U_r = -U \cos \theta \left( 1 - \frac{R^3}{r^3} \right) \quad (2)$$

$$U_\theta = U \sin \theta \left( 1 + \frac{R^3}{2r^3} \right) \quad (3)$$

The following simplifications result from the underlying assumptions: (*a*) The last term, IV, representing conduction in the $\theta$ direction is eliminated. (*b*) Expansion of the third term yields:

$$\frac{1}{r^2} \frac{\partial}{\partial r} \left( r^2 \frac{\partial T}{\partial r} \right) = \frac{\partial^2 T}{\partial r^2} + \frac{2}{r} \frac{\partial T}{\partial r} \approx \frac{\partial^2 T}{\partial r^2}$$

since $\partial^2 T/\partial r^2$ is of the order of magnitude of $1/\delta^2$ and $(2/r)(\partial T/\partial r)$ of $1/\delta R$, the latter may normally be neglected, compared to the former, for $R \gg \delta$. From a physical point of view this means neglecting the curvature of the drop with respect to the radial conduction.

(c) $$\frac{U_\theta}{r} \frac{\partial T}{\partial \theta} \simeq \frac{U_\theta}{R} \frac{\partial T}{\partial \theta}$$

since $r/R \approx 1$.

Thus, equation (1) is reduced to:

$$U_r \frac{\partial T}{\partial r} + U_\theta \frac{1}{R} \frac{\partial T}{\partial \theta} = \alpha \frac{\partial^2 T}{\partial r^2} \quad (4)$$

Now by statement of the problem:

$$\frac{r - R}{R} = \frac{y}{R} \ll 1$$

and the velocity vectors may be approximated by:

$$U_r \approx -3U \frac{y}{R} \cos \theta \quad (5)$$

$$U_\theta \approx \frac{3}{2} U \sin \theta \quad (6)$$

substituting (5) and (6) in (4) yields:

$$-3U \frac{y}{R} \cos \theta \frac{\partial T}{\partial r} + \frac{3}{2} \frac{U}{R} \sin \theta \frac{\partial T}{\partial \theta} = \alpha \frac{\partial^2 T}{\partial r^2} \quad (7)$$

or

$$\sin \theta \frac{\partial T}{\partial \theta} - 2y \cos \theta \frac{\partial T}{\partial y} = M \frac{\partial^2 T}{\partial y^2} \quad (8)$$

where

$$M = \frac{2R\alpha}{3U}$$

The relevant boundary conditions are:

$$T = 0 \qquad y = \infty; \qquad \pi \geqslant \theta \geqslant 0 \quad (9a)$$

$$T = T_0 \qquad y = 0 \; ; \qquad \pi \geqslant \theta \geqslant \beta \quad (9b)$$

$$T = 0 \qquad \infty \geqslant y > 0 \; ; \qquad \beta \geqslant \theta \geqslant 0 \quad (9c)$$

Boundary condition (9c) derives from the fact that at the upper part of the drop the vapour phase constitutes an adiabatic insulating plane. Thus, at $\theta = \beta$ the temperature of the continuous liquid is $T_\infty = 0$.

Introducing two new variables:

$$\psi = y \sin^2 \theta \quad (10)$$

$$\varphi = \int_B^\theta \sin^3 \theta \, d\theta$$

$$= \frac{1}{3}\cos^3 \theta - \cos \theta - \frac{1}{3}\cos^3 \beta + \cos \beta \quad (11)$$

and their derivatives:

$$\frac{\partial T}{\partial y} = \frac{\partial T}{\partial \psi} \sin^2 \theta \quad (12)$$

$$\frac{\partial^2 T}{\partial y^2} = \frac{\partial^2 T}{\partial \psi^2} \sin^4 \theta \quad (13)$$

$$\frac{\partial T}{\partial \theta} = \frac{\partial T}{\partial \psi} 2y \sin \theta \cos \theta + \frac{\partial T}{\partial \varphi} \sin^3 \theta \quad (14)$$

in the differential equation (8) yields:

$$\frac{\partial T}{\partial \varphi} = M \frac{\partial^2 T}{\partial \psi^2} \quad (15)$$

with the corresponding boundary conditions:

$$T = 0 \; ; \qquad \psi = \infty; \qquad \varphi \geqslant 0 \quad (16a)$$

$$T = T_0 \; ; \qquad \psi = 0 \; ; \qquad \varphi \geqslant 0 \quad (16b)$$

$$T = 0 \; ; \qquad \infty \geqslant \psi > 0 \; ; \qquad \varphi \geqslant 0 \quad (16c)$$

Note that equations (15) and (16) are similar to the well-known equations obtained when solving for temperature distribution in a semi-infinite wall. Utilizing the Laplace transformation, the solution obtained is:

$$T = T_0 \operatorname{erfc} \frac{\psi}{2\sqrt{(M\varphi)}} \quad (17)$$

where

$$\operatorname{erfc} X = 1 - \frac{2}{\Pi} \int_0^X \exp(X^2) \, dX$$

Substituting $\psi$, $\varphi$ and $M$ in (17) gives the temperature distribution around the drop:

$$T = T_0 \operatorname{erfc} \frac{y \sin^2 \theta}{2\left[\frac{2R\alpha}{3U}\left(\frac{1}{3}\cos^3 \theta - \cos \theta - \frac{1}{3}\cos^3 \beta + \cos \beta\right)^{0.5}\right]} \quad (19)$$

*Determination of heat-transfer coefficients*

The local heat flux per unit area, $q_\theta$, is conveniently obtained from equation (17). Thus:

$$q_\theta = -k\left(\frac{\partial T}{\partial y}\right)_{y=0} = -k\left(\frac{\partial T}{\partial \psi}\right)\left(\frac{\partial \psi}{\partial y}\right)_{y=0}$$

$$= k \frac{T_0}{\sqrt{(\pi)}} \frac{\sin^2 \theta}{(M\varphi)^{0.5}} \quad (20)$$

If the local heat-transfer coefficient $h$ is defined by:

$$h_\theta = \frac{q_\theta}{T_0} \quad (21)$$

then the local Nusselt number is given by:

$$Nu_\theta = \frac{3}{\sqrt{(\pi)}} (Pe)^{0.5} \frac{\sin^2 \theta}{(\cos^3 \theta - 3\cos \theta - \cos^3 \beta + 3\cos \beta)^{0.5}} \quad (22)$$

where:

$$Pe = Re \, . \, Pr = \frac{UD}{\alpha}$$

The numerical value of the local Nusselt number as a function of $\theta$ is given in Fig. 4 for four values of the opening angle of $\beta$.

The average heat flux per unit area of the drop may be calculated from:

$$q = \frac{1}{4\pi R^2}\int_{\beta}^{\Pi} q_\theta\, 2\pi R^2 \sin\theta\, \mathrm{d}\theta = \frac{kT_0}{2(\pi M)^{0.5}}$$

$$\int_{\beta}^{\pi} \frac{\sin^3\theta}{(\varphi)^{0.5}}\,\mathrm{d}\theta = \frac{kT_0}{2\pi M}\int_{0}^{\cos\beta - 1/3\cos^3\beta + 2/3} \frac{\mathrm{d}\varphi}{\sqrt{(\varphi)}}$$

$$= \frac{kT_0}{\sqrt{(\pi M)}}\sqrt{\left(\cos\beta - \frac{1}{3}\cos^3\beta + \frac{2}{3}\right)} \qquad (23)$$

With the average heat-transfer coefficient $h$ defined as:

$$h = \frac{q}{T_0} \qquad (24)$$

the average Nusselt number is:

$$Nu = \frac{hD}{k} = \left(\frac{3\cos\beta - \cos^3\beta + 2}{\pi}\right)^{0.5} (Pe)^{0.5}$$

$$= a\,.\,Pe^{0.5} \qquad (25)$$

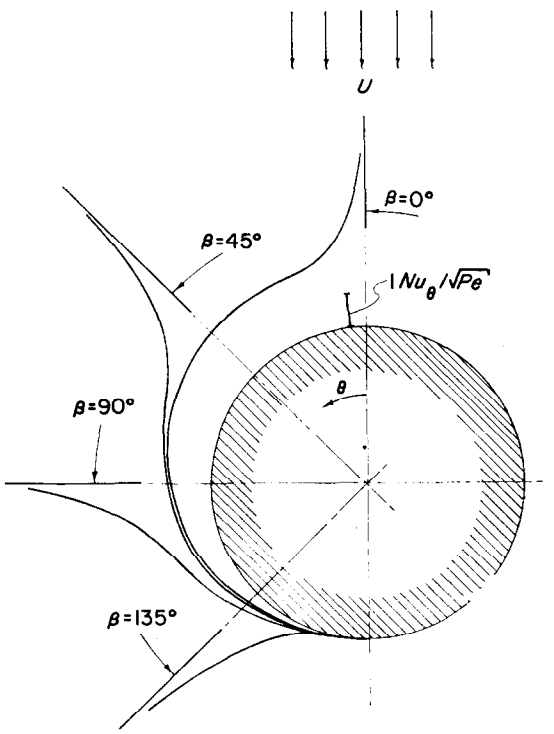


FIG. 4. Local Nusselt number for various values of the vapour opening angle.

The dependence of the average Nusselt number on $\beta$ is shown in Fig. 5. As is to be expected, the Nusselt number decreases with increasing $\beta$. Note that for $\beta = 0$ equation (25) reduces to the well-known equation obtained by Boussinesq [8] for potential flow around a sphere and by Higbie's [9] penetration theory, namely, $Nu = 1{\cdot}13\ (Pe)^{0.5}$ or $a = 1{\cdot}13$.

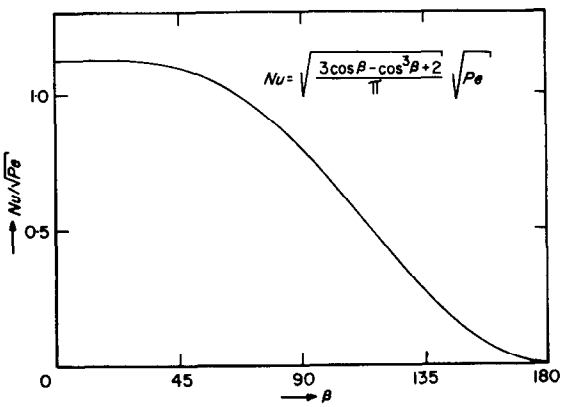


FIG. 5. Average Nusselt number as a function of the vapour opening angle.

## APPARATUS

The experimental apparatus (Figs. 6 and 7) consisted of a double-wall vacuum insulated glass column, 54 mm inside diameter, with top and bottom Perspex plates. To minimize visual distortions the column was placed in a square Perspex container filled with water, thus reducing the horizontal distortion from 1·3 to about 1·003. Single butane or pentane drops were introduced through a jacketed Perspex nozzle set in the bottom plate (Fig. 8). By circulating cooling liquids through the jacket of the nozzle, the volatile liquid was insulated from the hotter water in the column and the temperature of the drops could be controlled. A fine thermocouple (40 s.w.g. copper–constantan), inserted at the outlet of the nozzle, permitted determination of initial drop temperature. Water temperature was determined by another copper–constantan thermocouple mounted near the outlet of the nozzle and checked by a calibrated mercury glass thermometer immersed in the column.

The drops were photographed with a Paillard-Bolex H-16 Reflex ciné-camera, 56 frames/s,

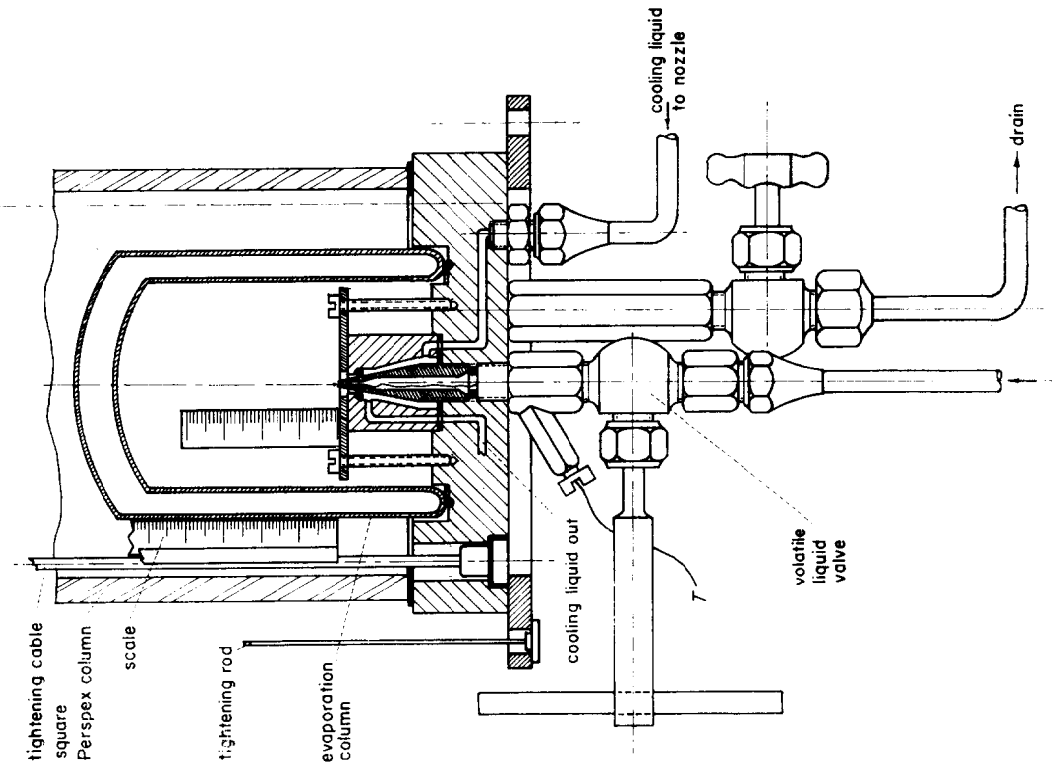


FIG. 8. Lower base and nozzle assembly.

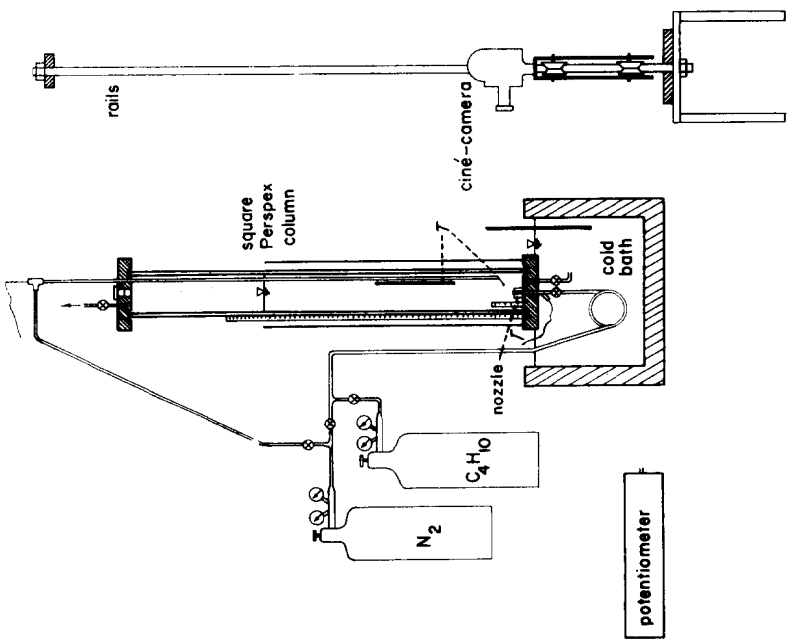


FIG. 7. Schematic diagram of apparatus, butane/water system.

1:2·8 lens, 75 mm focal length with a 10 mm extension tube. A special stand moving on vertical rails permitted the drops to be followed with the camera along the column. Whereas the vapour phase could be observed without special illumination, back lighting through a horizontal grid allowed better observation of the volatile liquid phase in the "drop" [10]. From the analysis of the consecutive pictures of each run, the heat flux to the "drop" (based on vapour volume) and the area and velocity of the drop could be conveniently determined at various evaporation stages.

## EXPERIMENTAL RESULTS AND ANALYSIS

Data were obtained by direct measurement of enlarged ($\times$ 20) consecutive pictures developed from the ciné-camera films. The heat input to the "drops" (determined by measuring the volume of the vapour), the area of the "drop" and its level at various times were calculated, plotted and correlated. (For these measurements the entire "drop" as well as the vapour phase were taken as spheroids). Figures 9, 10 and 11 illustrate the dependence of the heat input, "drop" area and "drop" level as function of time. Similar plots were drawn for all runs. These were correlated, yielding the following equations:

$$Q - Q_0 = Ct^n \tag{26}$$

$$A - A_0 = Kt^m \tag{27}$$

$$H - H_0 = Bt^p \tag{28}$$

where $Q_0$, $A_0$ and $H_0$ are the heat capacity, area and level at the beginning of the run, respectively. The constants $C$, $K$, $B$, $m$, $n$ and $p$ are given in Tables 1–4 for the various runs. It should be noted that equation (26) and (27) apply above 1 per cent evaporation, since the data below this evaporation ratio are uncertain due to end effects (drop formation), sub-cooling or superheating. These end effects do not apparently affect the dependence of the drop level on time, [equation (28)], above 0·1 per cent evaporation.

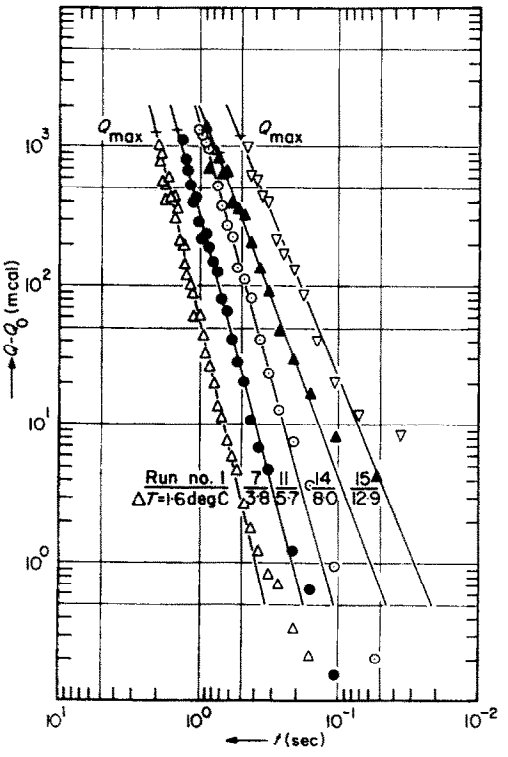


FIG. 9. Total heat input to drop vs. time.

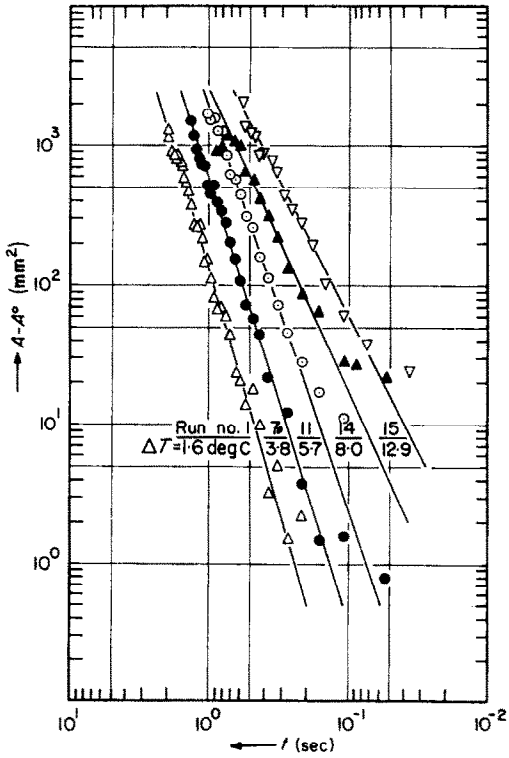


FIG. 10. Total area of drop vs. time.

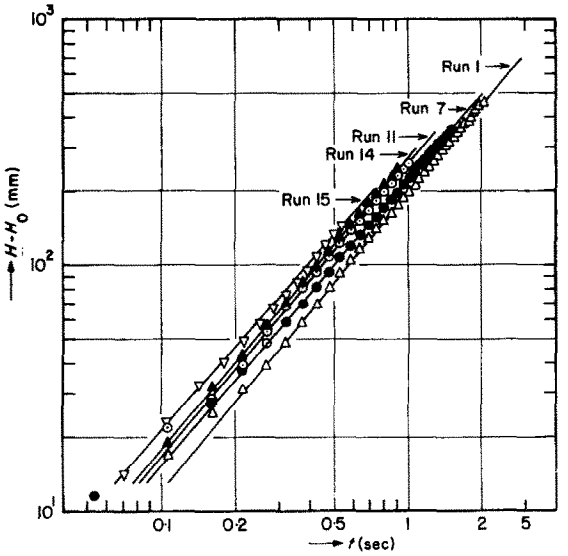


FIG. 11. Drop level vs. time.

*Table* 1. *Experimental results and correlation constants—pentane/distilled-water*

| | | | | | $Q = Ct^n + Q_0$ | | | $A = Kt^m + A_0$ | | | | | $H = Bt^p + H_0$ | | |
|---|---|---|---|---|---|---|---|---|---|---|---|---|---|---|---|
| Run No. | $\Delta T$ (deg C) | $d^*$ (mm) | $A^*$ (mm$^2$) | $Q_{max}$ (mcal) | $C$ | $n$ | $Q_0$ | $K$ | $m$ | $A_0$ | $t_v$ (s) | $H_v$ (mm) | $B$ | $p$ | $H_0$ |
| 1 | 1·6 | 3·60 | 40·8 | 1270 | 58 | 4·33 | 0·123 | 136 | 3·41 | 41·4 | 2·05 | 468 | 195 | 1·20 | 7 |
| 2 | 1·6 | 3·71 | 43·3 | 1390 | 66 | 4·10 | 0·100 | 142 | 3·63 | 43·6 | 2·11 | 545 | 220 | 1·20 | 6 |
| 3 | 1·9 | 3·63 | 41·3 | 1300 | 56 | 3·79 | 0·195 | 133 | 2·81 | 42·3 | 2·29 | 585 | 215 | 1·20 | 5 |
| 4 | 1·9 | 3·56 | 40·0 | 1234 | 44 | 3·87 | 0·195 | 115 | 3·17 | 40·7 | 2·36 | 553 | 200 | 1·18 | 5 |
| 5 | 3·7 | 3·42 | 37·7 | 1125 | 200 | 3·93 | 0·017 | 400 | 3·17 | 37·9 | 1·55 | 360 | 210 | 1·225 | 5·5 |
| 6 | 3·8 | 3·55 | 39·6 | 1218 | 265 | 4·27 | 0·070 | 480 | 3·37 | 40·0 | 1·43 | 323 | 205 | 1·21 | 6 |
| 7 | 3·8 | 3·62 | 41·2 | 1290 | 320 | 3·75 | 0·040 | 600 | 3·18 | 41·5 | 1·45 | 349 | 223 | 1·16 | 7 |
| 8 | 5·5 | 3·69 | 42·7 | 1350 | 777 | 3·53 | 0·096 | 1230 | 2·66 | 43·0 | 1·17 | 289 | 236 | 1·095 | 7 |
| 9 | 5·5 | 3·68 | 42·1 | 1340 | 1172 | 3·16 | 0·197 | 1600 | 2·54 | 43·1 | 1·04 | 269 | 250 | 1·075 | 6 |
| 10 | 5·7 | 3·62 | 41·3 | 1300 | 670 | 3·31 | 0·197 | 960 | 2·57 | 41·6 | 1·22 | 284 | 223 | 1·185 | 5 |
| 11 | 5·7 | 3·49 | 38·3 | 1105 | 1450 | 3·61 | 0·269 | 2000 | 2·91 | 38·3 | 0·935 | 243 | 259 | 1·18 | 5 |
| 12 | 8·0 | 3·50 | 38·4 | 1165 | 2950 | 2·99 | 0·198 | 2810 | 2·15 | 39·3 | 0·733 | 180 | 245 | 1·08 | 7 |
| 13 | 8·0 | 3·62 | 41·5 | 1220 | 2560 | 2·51 | 0·387 | 3110 | 2·00 | 41·5 | 0·742 | 199 | 260 | 1·048 | 7·5 |
| 14 | 8·0 | 3·20 | 32·2 | 895 | 1960 | 2·67 | 1·03 | 2670 | 2·16 | 36·9 | 0·745 | 202 | 278 | 1·185 | 5 |
| 15 | 12·9 | 3·52 | 39·0 | 1190 | 5700 | 2·43 | 2·15 | 5700 | 1·85 | 47·8 | 0·525 | 148 | 288 | 1·13 | 7 |
| 16 | 12·9 | 3·34 | 34·9 | 1010 | 6500 | 2·50 | 0·594 | 6000 | 1·98 | 37·6 | 0·475 | 122 | 300 | 1·265 | 4·5 |
| 17 | 14·5 | 3·30 | 34·3 | 989 | 22300 | 2·88 | 0·78 | 13230 | 2·16 | 37·9 | 0·339 | 79 | 253 | 1·133 | 5·5 |
| 18 | 14·5 | 3·36 | 35·5 | 1034 | 16200 | 2·75 | 0·834 | 13200 | 2·20 | 39·2 | 0·358 | 84 | 243 | 1·102 | 5·5 |

*Table 2. Experimental results and correlation constants—pentane/sea water*

| | | | | | $Q = Ct^n + Q_0$ | | | $A = Kt^m + A_0$ | | | | | $H = Bt^p + H_0$ | | |
|---|---|---|---|---|---|---|---|---|---|---|---|---|---|---|---|
| Run No. | $\Delta T$ (deg C) | $d^*$ (mm) | $A^*$ (mm²) | $Q_{max}$ (mcal) | $C$ | $n$ | $Q_0$ | $K$ | $m$ | $A_0$ | $t_v$ (s) | $H_v$ (mm) | $B$ | $p$ | $H_0$ |
| 21 | 2·4 | 3·85 | 46·7 | 1555 | 204 | 3·46 | 0·001 | 395 | 3·02 | 47·4 | 1·80 | 457 | 238 | 1·09 | 5 |
| 22 | 2·4 | 3·79 | 45·0 | 1480 | 195 | 3·29 | 0·087 | 400 | 2·53 | 45·1 | 1·85 | 449 | 228 | 1·085 | 5 |
| 23 | 4·6 | 3·80 | 45·2 | 1490 | 1070 | 3·12 | 0·196 | 1300 | 2·26 | 46·3 | 1·11 | 281 | 248 | 1·11 | 5·5 |
| 24 | 4·6 | 3·76 | 44·6 | 1455 | 1070 | 3·23 | 0·165 | 1430 | 2·51 | 45·3 | 1·10 | 280 | 248 | 1·15 | 5·5 |
| 25 | 5·8 | 3·82 | 45·9 | 1525 | 1820 | 3·38 | 0·045 | 2400 | 2·64 | 46·0 | 0·94 | 238 | 250 | 1·17 | 5 |
| 26 | 5·9 | 3·82 | 43·6 | 1410 | 1870 | 3·02 | 0·060 | 2450 | 2·43 | 43·6 | 0·91 | 242 | 265 | 1·155 | 5 |
| 27 | 6·6 | 3·80 | 45·4 | 1495 | 2230 | 3·11 | 1·07 | 2470 | 2·53 | 47·1 | 0·88 | 215 | 240 | 1·095 | 4 |
| 28 | 6·6 | 3·77 | 44·7 | 1465 | 3100 | 2·49 | 0·712 | 3200 | 1·90 | 47·6 | 0·74 | 209 | 283 | 1·05 | 4 |
| 29 | 7·9 | 3·82 | 45·7 | 1515 | 3050 | 2·41 | 0·069 | 3750 | 2·00 | 46·0 | 0·748 | 192 | 260 | 1·11 | 5 |
| 30 | 11·1 | 3·91 | 48·2 | 1635 | 6200 | 2·21 | 0·217 | 6100 | 1·76 | 49·4 | 0·547 | 138 | 255 | 1·08 | 7 |
| 31 | 11·1 | 3·95 | 49·1 | 1680 | 6000 | 1·86 | 3·16 | 4900 | 1·38 | 60·6 | 0·505 | 148 | 265 | 0·94 | 12·5 |

*Table 3. Experimental results and correlation constants—butane/sea water*

| | | | | | $Q = Ct^n + Q_0$ | | | $A = Kt^m + A_0$ | | | | | $H = Bt^p + H_0$ | | |
|---|---|---|---|---|---|---|---|---|---|---|---|---|---|---|---|
| Run No. | $\Delta T$ (deg C) | $d^*$ (mm) | $A^*$ (mm²) | $Q_{max}$ (mcal) | $C$ | $n$ | $Q_0$ | $K$ | $m$ | $A_0$ | $t_v$ (s) | $H_v$ (mm) | $B$ | $p$ | $H_0$ |
| 41 | 4·1 | 3·80 | 45·4 | 1585 | 590 | 2·25 | 0·12 | 880 | 1·87 | 50 | 1·55 | 368 | 228 | 1·060 | 6 |
| 42 | 4·2 | 3·86 | 46·7 | 1650 | 510 | 2·81 | 0·05 | 900 | 2·47 | 50 | 1·52 | 367 | 234 | 1·025 | 6 |
| 43 | 4·2 | 3·80 | 45·4 | 1585 | 560 | 2·80 | 0·02 | 840 | 2·26 | 50·2 | 1·45 | 348 | 236 | 1·015 | 6 |
| 44 | 6·7 | 3·40 | 36·5 | 1132 | 940 | 2·77 | 0·18 | 1280 | 2·17 | 37·7 | 1·07 | 260 | 234 | 1·04 | 6 |
| 45 | 6·7 | 3·40 | 36·5 | 1132 | 1280 | 2·23 | 0·62 | 1700 | 1·70 | 45·0 | 0·95 | 255 | 265 | 1·08 | 6 |
| 46 | 9·4 | 3·40 | 36·3 | 1126 | 1320 | 2·21 | 0·11 | 1700 | 1·67 | 40·5 | 0·93 | 241 | 252 | 1·09 | 6 |
| 47 | 9·4 | 3·39 | 36·2 | 1120 | 2180 | 2·17 | 0·20 | 2900 | 1·70 | 38·0 | 0·74 | 191 | 257 | 1·06 | 6 |
| 48 | 12·5 | 3·48 | 38·2 | 1165 | 3600 | 1·92 | 0·37 | 3800 | 1·45 | 41·0 | 0·55 | 143 | 250 | 1·025 | 6 |
| 49 | 12·5 | 3·40 | 36·3 | 1135 | 3350 | 2·01 | 0·02 | 4300 | 1·67 | 40·0 | 0·58 | 159 | 276 | 1·08 | 6 |
| 50 | 12·5 | 3·35 | 35·3 | 1082 | 2900 | 2·00 | 1·13 | 3250 | 1·62 | 45·0 | 0·61 | 180 | 295 | 1·09 | 6 |

The temperature difference is not the only condition required for the evaporation of the drops in the continuous medium. Evaporation starts only after nucleation has set in in the drop. At a given temperature difference the onset of nucleation usually depends on external disturbances and the degree of impurity of the liquids involved. With highly pure systems the limit of superheat was found [11, 12] to be above 100°C. This study showed that impurities in the volatile liquid and contamination normally associated with sea water, as well as very small gas bubbles introduced by mechanical mixing, are factors which retard superheating and promote nucleation. Since the object of this work was the study of heat-transfer characteristics during evaporation rather than that of the superheat phenomenon, nucleation was sometimes induced by allowing minute amounts of air to dissolve in the volatile liquid, or by introducing small (below 0·1 mm) gas bubbles into the continuous medium. Note that under normal

*Table 4. Experimental results and correlation constants—pentane/sea water (small drops)*

| | | | | | $Q = Ct^n + Q_0$ | | | $A = Kt^m + A_0$ | | | | | $H = Bt^p + H_0$ | | |
|---|---|---|---|---|---|---|---|---|---|---|---|---|---|---|---|
| Run No. | $\Delta T$ (deg C) | $d^*$ (mm) | $A^*$ (mm$^2$) | $Q_{max}$ (mcal) | $C$ | $n$ | $Q_0$ | $K$ | $m$ | $A_0$ | $t_v$ (s) | $H_v$ (mm) | $B$ | $p$ | $H_0$ |
| 61 | 0·8 | 1·94 | 11·25 | 198 | 112 | 3·39 | 0·047 | 285 | 2·58 | 12·17 | 1·183 | 271 | 220 | 1·15 | 3 |
| 62 | 0·9 | 1·965 | 12·15 | 207 | 75 | 3·52 | 0·024 | 200 | 2·57 | 12·17 | 1·334 | 314 | 220 | 1·19 | 5 |
| 63 | 3·4 | 1·965 | 12·15 | 207 | 245 | 2·25 | 0 | 480 | 1·66 | 12·17 | 0·93 | 213 | 226 | 1·095 | 4 |
| 64 | 7·1 | 1·995 | 12·5 | 216 | 4600 | 2·34 | 0 | 6100 | 1·905 | 12·31 | 0·270 | 60 | 270 | 1·145 | 1·5 |
| 65 | 7·2 | 1·995 | 12·5 | 216 | 5000 | 2·23 | 0 | 6500 | 1·78 | 12·58 | 0·244 | 55 | 231 | 1·03 | 2 |
| 66 | 7·6 | 1·995 | 12·5 | 216 | 3900 | 2·19 | 0 | 5200 | 1·73 | 12·58 | 0·267 | 63 | 290 | 1·17 | 2 |
| 67 | 10·6 | 2·0 | 12·57 | 218 | 14000 | 2·58 | 0 | 12600 | 1·985 | 12·56 | 0·199 | 42 | 300 | 1·24 | 2·5 |
| 68 | 10·8 | 1·965 | 12·15 | 207 | 12500 | 2·41 | 0 | 15000 | 1·97 | 12·17 | 0·182 | 41 | 296 | 1·195 | 3 |
| 69 | 11·0 | 2·0 | 12·57 | 218 | 10300 | 2·15 | 0 | 12300 | 1·765 | 12·56 | 0·168 | 38 | 271 | 1·135 | 3 |
| 70 | 12·8 | 2·0 | 12·57 | 218 | 27200 | 2·51 | 0 | 23000 | 2·01 | 12·56 | 0·146 | 30 | 278 | 1·18 | 2 |
| 71 | 13·0 | 1·995 | 12·5 | 216 | 24100 | 2·45 | 0 | 16500 | 1·84 | 12·58 | 0·146 | 30 | 320 | 1·25 | 2·5 |
| 72 | 14·4 | 2·0 | 12·57 | 218 | 38000 | 2·54 | 0 | 25000 | 1·94 | 12·56 | 0·131 | 28 | 272 | 1·145 | 2 |
| 73 | 15·5 | 1·965 | 12·15 | 207 | 19200 | 2·08 | 0 | 21700 | 1·74 | 12·17 | 0·113 | 26 | 238 | 1·055 | 2 |
| 74 | 15·6 | 1·965 | 12·15 | 207 | 55000 | 2·47 | 0 | 25500 | 1·815 | 12·17 | 0·104 | 24 | 264 | 1·095 | 2 |

industrial operating conditions such induced nucleation will not be warranted.

(a) *Time and level of total evaporation*

The time required for the complete evaporation of the drop can be obtained from equation (26), where $Q$ is independently calculated from the initial volume of the drop and the latent heat of vaporization. Thus, for $Q = Q_{max}$:

$$t_v \simeq \left(\frac{Q_{max}}{C}\right)^{1/n} \tag{29}$$

Direct visual determination of the end of the evaporation from the films closely agree with the values obtained from equation (29).

The height required for total evaporation can be determined either by equation (28) where $t = t_v$, or by direct observation.

The results shown in Figs. 12 and 13 clearly indicate that the maximum evaporation time and level decrease with increasing temperature difference and vice versa, with the co-ordinates as the asymptotic values. The accuracy of these plots is estimated at $\pm 10$ per cent.

The values obtained for the various systems (butane/sea water, pentane/distilled water and pentane/sea water) are quite similar. Quite different results (not included here) were obtained with butane/distilled water system. This is most probably due to the freezing of the water layer adjoining the subcooled (below 0°C) butane drops.

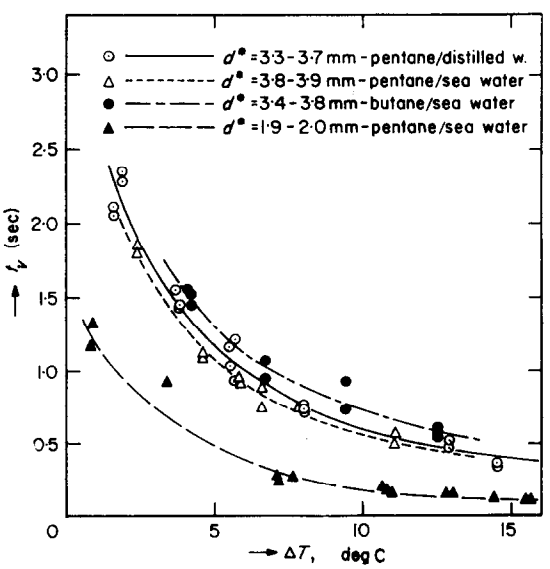


FIG. 12. End of evaporation time vs. $\Delta T$.

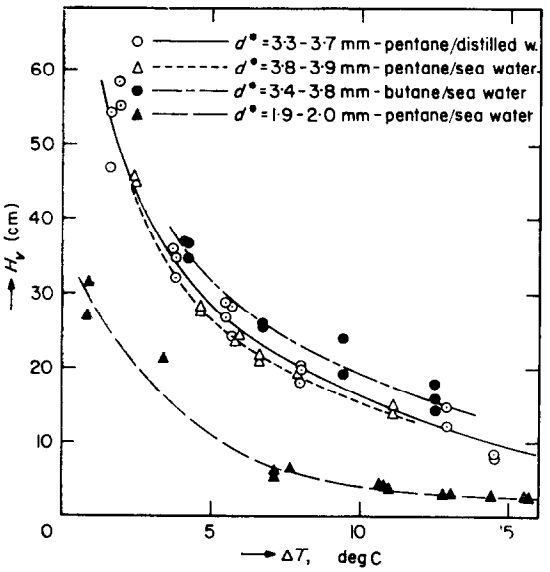


FIG. 13. End of evaporation height vs. $\Delta T$.

(b) *Drop velocity*

The velocity of the rising evaporating drop increases with vapour phase growth. The instantaneous velocity, $U$, as a function of the evaporation ratio may be obtained by differentiating equation (28):

$$U = \frac{dH}{dt} = Bpt^{p-1} \tag{30}$$

and since the evaporation ratio $\xi$ is given by:

$$\xi = \frac{G_v}{G} = \frac{Q}{Q_{max}} = \frac{Ct^n + Q_0}{Q_{max}} \simeq \frac{Ct^n}{Q_{max}} \tag{31}$$

substitution of (31) in (30) yields:

$$U = Bp\left(\frac{\xi Q_{max}}{C}\right)^{p-1/n} \tag{32}$$

The dependence of the velocity on the vaporization ratio, based on the average of all runs, is given in Fig. 14. The accuracy of these data is estimated as $\pm 10$ per cent. The dependence of the average velocity on the temperature difference is illustrated in Fig. 15, where the arithmetic mean of the velocities of drops with 1 and 100 per cent evaporation was taken. These averages were also used in the subsequent heat-transfer calculations. It is seen that the temperature effect on the average velocity is relatively small. This may probably be explained by the fact that the vapour phase growth is "slow" enough to allow for a quasi-equilibrium between drag forces and buoyancy. With smaller drops, however, where the rate of growth is much faster (resembling an explosion to the naked eye) the velocity was found to decrease slightly with increase of $\Delta T$.

(c) *Heat-transfer coefficient related to initial drop diameter*

The heat-transfer coefficient per unit area of initial liquid drop is defined as:

$$h_m^* = \frac{q'}{A^* \Delta T} \tag{33}$$

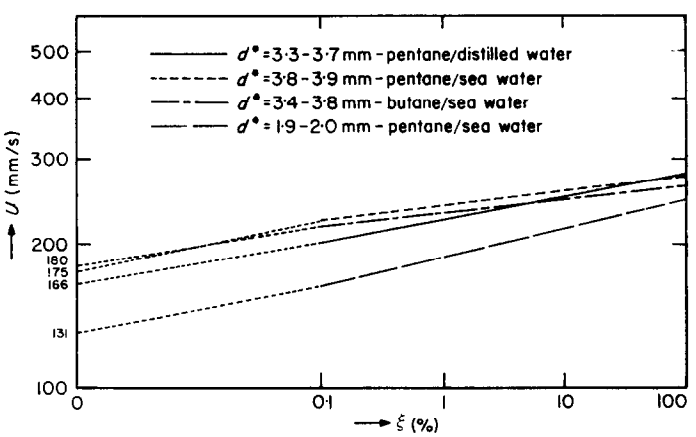


FIG. 14. Velocity of evaporating drop vs. $\xi$.

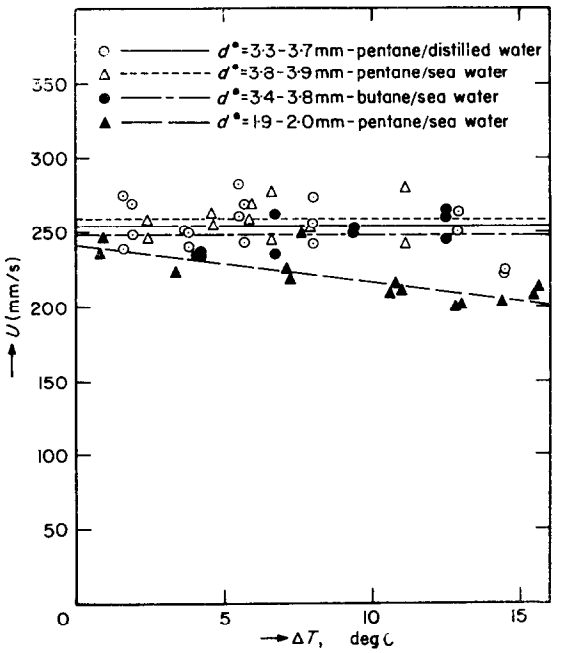


FIG. 15. Average velocity of evaporating drop vs. $\Delta T$.

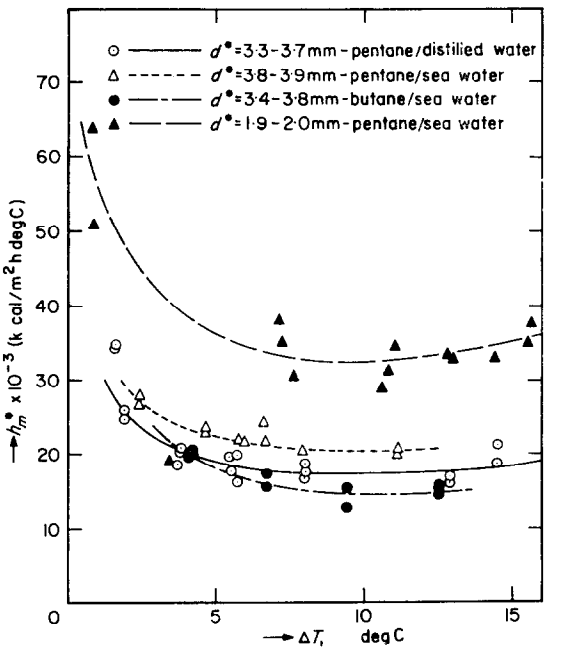


FIG. 16. Average overall heat transfer coefficients.

and given by:

$$h_m^* = \frac{Q_{\max}}{t_v A^* \Delta T}\left[\frac{m\ \text{cal}}{\text{mm}^2\ \text{s degC}}\right] = \frac{3600 C t_v^{n-1}}{\Delta T A^*}\left[\frac{\text{kcal}}{\text{m}^2\ \text{h degC}}\right] \quad (34)$$

where $A^*$ is the area of the initial liquid drop. Though somewhat artificial, the definition permits practical use of this coefficient, since the initial drop diameter is usually known and/or can be determined in advance [13, 14].

Figure 16 illustrates that in the range of 3° to 15°C the heat-transfer coefficient $h_m^*$ is almost independent of the temperature difference. The sharp increase of $h_m^*$ with the temperature difference below 3°C should be considered with reservations, due to the limited accuracy of the measurements in this range. Note that $\Delta T$ is defined as the difference between the average temperatures of the water and the liquid drop, where the average of the column top and bottom boiling points was taken as the temperature of the drop. The effect of the hydrostatic head is greater, the lower $\Delta T$. Also, the true temperature difference decreases as the drop rises. Thus, the average used here is not truly representative since it yields lower apparent "$\Delta T$'s" which, when introduced in equation (34), yields higher values of $h_m^*$.

Comparison of the coefficients for heat transfer from drops with and without change of phase indicate the advantages of utilizing the former for heat-transfer operations. While for non-evaporating drops the coefficient is about 300 kcal/m² h degC, the values for the same initial drop diameter (3·5 mm) obtained in the present investigation are about 20000 kcal/m² h degC.

(d) *Instantaneous heat-transfer coefficient related to actual drop area*

Although not conveniently applicable for design purposes, the transfer coefficient as defined below allows for better description and understanding of the physical phenomenon and lends itself to theoretical analysis. By definition:

$$h = \frac{q'}{A\Delta T} \quad (35)$$

where $A$ is the envelope area of the "drop" at any instant. Substituting in (35) the derivative of equation (26) for $q$, the area from equation (27) and time from equation (31) we have:

$$h = \frac{3600nC\left(\frac{Q_{\max}}{C}\right)^{n-1/n}}{\Delta T A_0} \frac{\xi^{n-1/n}}{\frac{K}{A0}\left(\frac{Q_{\max}}{C}\right)^{m/n}\xi^{m/n}+1} \quad (36)$$

The dependence of $h$ on $\xi$, the vaporization ratio, is illustrated in Fig. 17 for various temperature differences and drop diameters. It can be seen that the heat-transfer coefficient increases rapidly up to about 3–5 per cent evaporation, reaching its maximum value, and then decreases gradually. The curves in Fig. 17 actually represent the average values obtained from several runs under identical operating conditions, as calculated from Tables 1–4. It is estimated that for the 3·5–4·0 mm drop diameter the accuracy of the data is approximately ±15 per cent, whereas for the smaller drop (~2 mm) it is approximately ±20 per cent.

## DISCUSSION

It is assumed that the temperature at the vapour–liquid interphase inside the drop is that of the boiling point corresponding to the proper vapour pressure. As the liquid layer at the bottom of the drop becomes thinner, the main portion of heat penetrates through this layer, whose resistance is very much less than that of the vapour phase. Thus, the sharp increase of $h$ in the first stages of evaporation (up to about 3–5 per cent) corresponds to the decrease in thickness of the volatile liquid, i.e. of the internal resistance to heat transfer. The maximum heat-transfer coefficient is obtained when the liquid layer is thin enough and the internal resistance to transfer negligible compared with its external counterpart. This occurs between 3 to 10 per cent evaporation, depending on operating conditions. The moderate decrease in the transfer coefficient beyond this maximum may correspond to the gradual reduction in the relative liquid area. Unfortunately, this process can only be observed at the beginning (up to about 10 per cent), since at higher vapour ratios the liquid layer is so thin as to become invisible. However, it is logical to assume that the reduction in

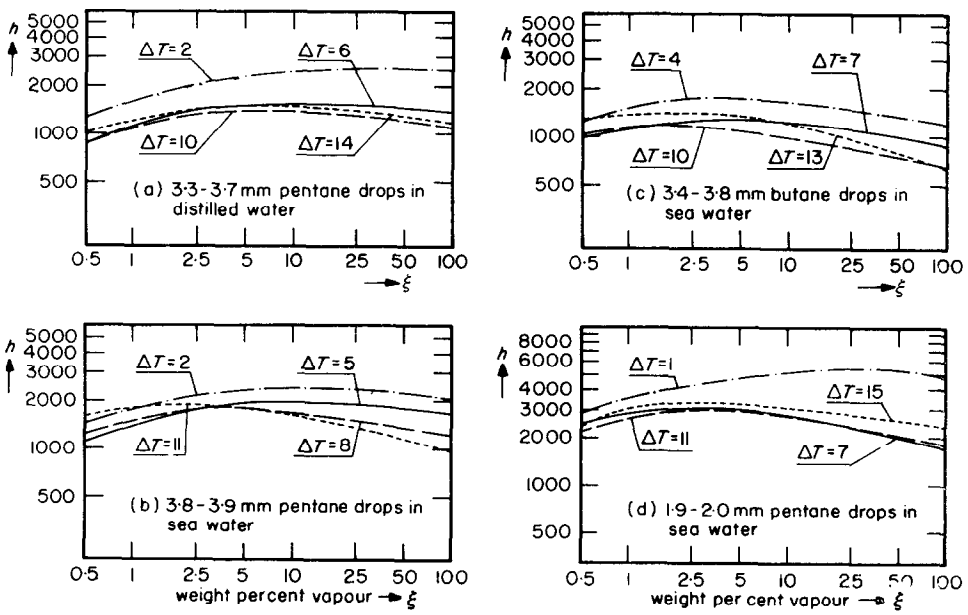


FIG. 17. Overall instantaneous heat-transfer coefficients ($h$ in kcal/m² h degC).

relative area continues within the invisible region as well.

These ideas are associated with the mathematical model of the evaporating drop, where the volatile liquid is assumed isothermal and of negligible internal resistance and the vapour resistance infinite. Thus, assumption of a constant temperature, $T_0$, in the volatile liquid is more valid the thinner the layer. Obviously, comparison between the theoretical model and experiment can presently be attempted only in the 3 to 10 per cent range, where the volatile layer is thin enough to justify neglect of the internal resistance, yet still sufficiently visible to permit measurement.

Table 5 presents the calculated opening angles of the liquid phase ($\epsilon = 360 - 2\beta$) based on the theory developed [equation (25)] and using the experimental values for the Nusselt numbers from the $h$ vs. $\xi$ curves (Fig. 17). It is important to note that the opening angle $2\beta$, as seen in the ciné-camera pictures, is about 180° at 1 per cent evaporation and increases up to about 270° in the 3 to 10 per cent range (Fig. 18). Although no visual observation is possible above that range, it is assumed that reduction of the angle above the observed range is quite moderate, corresponding to the gradual decrease of the heat-transfer coefficient. Thus, at first approximation, good maximum values may be obtained, if the angle is taken at 135°.

It is evident from Fig. 4 that the local heat-transfer coefficient $h_\theta$ is infinite at $\theta = \beta$, decreasing rapidly at first with increasing $\theta$ and then moderately to zero as $\theta \to 180°$. This is as expected, since the temperature gradient at $\theta = \beta$ tends to infinity. However, since this effect is limited to a narrow region of $\theta \cong \beta$, the average heat-transfer coefficient (per unit total area of the drop) is only slightly affected by this singularity. Obviously, the higher the opening angle, the lower the average heat-transfer coefficient (Fig. 5).

A number of assumptions and simplifications leading to the analytical solution call for further elucidation and discussion.

*Table 5. Calculated values of the opening angle*

| No. | System | Initial drop diameter $D^*$ (mm) | Temp. drop $\Delta T$ (degC) | Evaporation ratio $\xi$ (%) | Heat-transfer coefficient $h$ (kcal/m²h degC) | Equivalent diameter $D \approx \sqrt[3]{\left(\frac{\rho_L}{\rho_v}\xi\right)} D^*$ (mm) |
|---|---|---|---|---|---|---|
| 1 | Pentane–distilled water | 3·6 | 6 | 10 | 1550 | 9·8 |
| 2 | Pentane–sea water | 3·9 | 5 | 10 | 1950 | 10·6 |
| 3 | Pentane–sea water | 2·0 | 7 | 3 | 3100 | 3·7 |
| 4 | Butane–sea water | 3·6 | 7 | 5 | 1300 | 7·9 |

| No. | Nusselt number $Nu$ | Drop velocity $U$ (mm/s) | Peclet number $Pe = \frac{UD}{\alpha}$ | $Nu/\sqrt{(Pe)}$ | Calculated $\beta$ (°) | Calculated $\epsilon\ (= 360 - 2\beta)$ |
|---|---|---|---|---|---|---|
| 1 | 28·1 | 254 | 16400 | 0·22 | 140 | 80 |
| 2 | 38·3 | 259 | 18100 | 0·285 | 134 | 92 |
| 3 | 21·3 | 225 | 5500 | 0·287 | 134 | 92 |
| 4 | 21·6 | 248 | 15000 | 0·177 | 145 | 70 |

(*a*) The smaller the drop, the better the assumption of spherical shape. However, with larger drops, above 2 mm in initial diameter, the drop is actually a spheroid and the assumption only yields an approximate result.

(*b*) Neglect of the drop growth rate compared with its relative velocity in the continuous medium permits steady-state treatment of the problem. Although this situation is approached at small temperature gradients, this assumption confines the treatment to stage-wise situations. It permits determination of the transfer coefficient at any moment, but on the other hand is time-independent.

(*c*) The relatively low thermal diffusivity and heat-transfer coefficient in the gas phase justify assumption of infinite resistance at the exposed vapour phase surface.

(*d*) Assumption of potential flow around the sphere (which, incidentally, is physically identical with Higbie's penetration theory) gives better results the higher the Reynolds number and the ratio of the viscosities of the continuous and drop phases. Ruckenstein [15] recently used this very assumption in his calculation of heat-transfer coefficients around a vapour bubble and reported good agreement with experimental results. Similarly, results within 20 per cent of the experimental ones were reported [16] for heat transfer to liquid drops of lower viscosities. Considering that the Reynolds numbers actually dealt with here are above 1000 and the viscosity ratio of liquid systems of practical interest (i.e. water–butane) is about 7, the potential flow assumption is reasonably accurate.

In spite of the limitations mentioned above, the analytical solution proposed here permits good approximation of the actual average heat-transfer coefficients. Good results may be obtained when $\beta$ is taken as a characteristic opening angle including correction factors for all the assumptions and simplifications involved in the analytical treatment. Based on our experiments with four systems (butane, pentane, sea and distilled water), it is suggested that $\beta$ be taken as 135° to obtain the maximum heat-transfer coefficients. The effect of the temperature difference on the transfer coefficient is generally small (Fig. 16) and the variation may be considered almost within the range of experimental error. This independence is consistent with equation (12) or any other theoretical derivation for forced convection. The sharp increase in the coefficient at lower $\Delta T$ is, most probably, due to the increasing effect of the hydrostatic head on the temperature difference.

## CONCLUSIONS

The photographic study of volatile liquid drops evaporating in an immiscible liquid medium elucidated the transfer characteristics and permitted the determination of some basic information regarding this unique heat-transfer process. In general, it was found that:

(*a*) The time and level of total drop evaporation are inversely proportional to the temperature difference between the dispersed and continuous media.

(*b*) The rising velocity of the "drop" is proportional to the evaporation ratio, increasing moderately above 1 per cent evaporation. The average velocity in this range is about 25 cm/s for $D^* = 3{\cdot}7$ mm and 22 cm/s for $D^* = 2{\cdot}0$ mm. The velocities of non-evaporating drops of corresponding diameters are 17·5 and 13 cm/s respectively.

(*c*) The heat-transfer coefficient related to the initial drop diameter $D^*$ is about 20 000 kcal/m$^2$ h degC for $D^* = 3{\cdot}5$–$4{\cdot}0$ mm and approaches 35 000 kcal/m$^2$ h degC for $D^* = 2{\cdot}0$. The corresponding coefficient for non-evaporating drops is about 300 kcal/m$^2$ h degC.

(*d*) The instantaneous heat-transfer coefficient related to the actual area of the rising "drop" increases sharply with the vaporization ratio up to 3–10 per cent (depending on system and conditions) and then decreases quite moderately until evaporation is complete. The orders of magnitude of the coefficients are 1000–2000 kcal/m$^2$ h degC for $D^* = 3{\cdot}5$ mm and 2500–3500 kcal/m$^2$ h degC for $D^* = 2{\cdot}0$ mm.

(*e*) The dependence of the heat-transfer coefficients on the temperature difference in the 4–15°C range is very weak. Below this range a marked increase in the coefficient is noted.

(*f*) Only small differences were found between the systems butane/sea water, pentane/distilled water and pentane/sea water. The butane/distilled water system indicated quite a different behaviour, probably due to the formation of ice around the cold butane drop.

(*g*) Nucleation and onset of evaporation are faster the larger the drops; they are better in sea water (compared with distilled water) and in the presence of impurities, small gas bubbles and mechanical mixing.

(*h*) The analytical solution obtained permits determination of the average heat-transfer coefficient as a function of the opening angle of the vapour phase and the Peclet number. It is in satisfactory agreement with the experiment and allows for better understanding of the phenomenon. It is suggested that with $\beta = 135°$, good approximation of the maximum heat-transfer coefficient may be obtained.

The work reported herein constitutes the first reported detailed study of this unique process of heat transfer. Nevertheless, the results obtained so far strongly favour its practical utilization.

## ACKNOWLEDGEMENT

The authors acknowledge, with thanks, the financial support of the Israel Research and Development Council. Thanks are also due to Dr. M. Bentwich of the Faculty of Mechanical Engineering, Technion—Israel Institute of Technology, for his stimulating discussions and help in obtaining the analytical solution, and to Dr. Z. Rotem of the same Faculty for his continued interest in, and long discussions on, this work. Thanks are also due to Mr. A. Golan of the Israel Water Desalination (Zarchin) Projects, for his helpful suggestions.

This paper forms part of the thesis submitted by Y. Taitel to the Senate of the Technion—Israel Institute of Technology, in partial fulfilment of its requirements for the M.Sc. degree.

## REFERENCES

1. S. SIDEMAN, Direct contact heat-transfer between single drops and immiscible liquid medium. Review, *Canad. J. Chem. Engng* **42**, 17 (1964).
2. S. UMANO, Direct-contact refrigeration, Japanese Gov. Chem. Ind. Res. Publication (in English), May (1959).
3. H. F. WIEGANDT, Saline water by direct freezing, Publication 568, 377, Nat. Academy of Science, Washington, D.C. (1958).
4. H. F. WIEGANDT, Saline water conversion by freezing, Office of Saline Water and Development, Progress Report No. 41, August (1960).
5. H. F. WIEGANDT, *Symposium on saline water conversion*, Cleveland, Ohio (1960).
6. G. KARNOFSKY and P. F. STEINHOFF, Saline water conversion by direct freezing with butane, Office of Saline Water Research and Development.
7. Y. TAITEL, Direct contact heat-transfer with a change of phase (evaporation), M.Sc. Thesis, Israel Institute of Technology, Haifa, 1963.
8. M. BOUSSINESQ, Calcul du pouvoir refroidissant des courants fluides, *J. Math. Pure Appl.* **1**, 285 (1905).
9. R. HIGBIE, The rate of absorption of a pure gas into a still liquid during short periods of exposure, *Trans.* **31**, 365 (1935).
10. S. SIDEMAN, Photography of drops in liquid media, *Chem. Engng Sci.* **xix**, 426 (1964).
11. H. WAKESHIMA and K. TAKATA, On the limit of superheat, *J. Phys. Soc. Japan* **13**, 1398 (1958).
12. G. R. MOORE, Evaporation of superheated drops in liquids, *J. Amer. Inst. Chem. Engrs* **5**, 458 (1959).
13. C. B. HAYWORTH and R. E. TREYBAL, Drop formation in two liquid–liquid phase systems, *Ind. Engng Chem.* **42**, 1174 (1950).
14. S. NORDBERG, Droplet formation in fluids (in German), *Dechema Monogr.* **41**, 257 (1962).
15. E. RUCKENSTEIN, On heat transfer between vapour in motion and the boiling liquid from which they are generated, *Chem. Engng Sci.* **10**, 22 (1959).
16. P. HARRIOTT, A review of mass transfer to interfaces, *Canad. J. Chem. Engng* **40**, 60 (1962).

**Résumé**—Les caractéristiques de transport de gouttes de liquide volatil qui s'évaporent tout en s'elevant dans une colonne d'un autre liquide non miscible sont présentées. Une étude de films cinématographiques pris pendant le processus le transporte de chaleur fournit une information concernant les vitesses et les taux d'evaporation de gouttes de butane et de pentane se vaporisant dans de l'eau de mer et de l'eau distillée. Les coefficients globaux de transport de chaleur rapportés à l'aire initiale de la goutte, et les coefficients instantanés de transport de chaleur rapportés à l'aire actuelle sont présentés. Ces derniers sont comparés avec une étude analytique de ce problème qui fournit l'équation:

$$Nu = \left(\frac{3\cos\beta - \cos^3\beta + 2}{\pi}\right)^{0,5} Pe^{0,5} = a\,Pe^{0,5}$$

pour le nombre de Nusselt moyen, où $2\beta$ est l'angle d'ouverture de la phase gazeuse dans la goutte. On suggère qu'avec $\beta = 135°$ ($a = 0{,}27$) une bonne approximation des coefficients maximaux de transport de chaleur peut être obtenue.

**Zusammenfassung**—Es werden die Wärmeübertragungseigenschaften von Tropfen einer flüchtigen Flüssigkeit angegeben, die beim Aufsteigen in einer damit nicht mischbaren Flüssigkeit verdampfen.

Filmaufnahmen von dem Wärmeübergangsprozess erbrachten Aufschlüsse über die Geschwindigkeit und die Verdampfungsraten von Butan- und Pentantropfen, die in Seewasser und destilliertem Wasser verdampfen. Der mittlere (gesamte) Wärmeübergangskoeffizient bezogen auf die anfängliche Oberfläche des flüssigen Tropfens und der momentane Wärmeübergangskoeffizient bezogen auf die momentane, wirkliche Flache, werden mitgeteilt. Letztere Ergebnisse werden verglichen mit einer theoretischen Untersuchung dieses Problems, die zu folgender Gleichung für die mittlere Nusselt-Zahl führt:

$$Nu = \left(\frac{3\cos\beta - \cos^3\beta + 2}{\pi}\right)^{0,5} Pe^{0,5} = a\,Pe^{0,5}$$

wobei $2\beta$ der Öffnungswinkel der Dampfphase (Blase) im Tropfen ist. Mit $\beta = 135°$ ($a = 0{,}27$) wird vermutlich eine gute Annäherung des maximalen Wärmeübergangskoeffizienten erreicht.

**Аннотация**—Приводятся характеристики переноса капель летучей жидкости, испаряющейся по мере подъема в столбике другой несмешивающейся жидкости. Изучение кинопленок, заснятых в процессе теплообмена, дает сведения о скорости движения и интенсивности испарения капель бутана и пентана в морской и дистиллированной воде. Представлены суммарные коэффициенты теплообмена, отнесенные к начальной площади капли жидкости, и мгновенные коэффициенты теплообмена, отнесенные к действительной площади.

Последние сравниваются с данными аналитического решения, которое дает уравнение:

$$Nu = \left(\frac{3\cos\beta - \cos^3\beta + 2}{\pi}\right)^{0,5} Pe^{0,5} = a\,Pe^{0,5}$$

для среднего значения критерия Нуссельта, где $2\beta$ есть телесный угол паровой фазы в капле. Высказано предположение, что при $\beta = 135°$ ($a = 0{,}27$) можно получить хорошую аппроксимацию максимальных коэффициентов теплообмена.